

# Surface Vibration Induced Spatial Ordering of Periodic Polymer Patterns on a Substrate

Mar Alvarez, James R. Friend, and Leslie Y. Yeo\*

*Micro/Nanophysics Research Laboratory, Monash University, Clayton, VIC 3800, Australia*

*Received July 15, 2008. Revised Manuscript Received September 4, 2008*

We demonstrate the possibility of producing regular, long-range, spatially ordered polymer patterns without requiring the use of physical or chemical templating through the interfacial destabilization of a thin polymer film driven by surface acoustic waves (SAWs). The periodicity and spot size of the pattern are observed to be dependent on a single parameter, that is, the SAW frequency (or wavelength), therefore offering a rapid, simple, yet novel method for self-organized regular spatial polymer pattern formation that is far more tunable than conventional polymer patterning procedures.

There has been recent interest in the microscale patterning of functional polymers onto surfaces for applications ranging from microelectronics and photonics to cell adhesion and protein patterning for tissue engineering and biosensor development. Besides photolithography and nanoimprint or micro/nanocontact printing techniques,<sup>1,2</sup> large-scale, organized patterning with control of the morphology can be achieved through local self-organizational processes such as the dewetting of thin polymer films.<sup>3–5</sup> Such dewetting is initiated either through the creation of nucleation sites<sup>6</sup> (for example, by chemical<sup>7</sup> or physical<sup>8</sup> substrate templating, which induces local gradients in the chemical potential or wettability) or by the destabilization of capillary waves triggered by electric, thermocapillary, or Marangoni stresses leading toward film rupture as a consequence of long-range intermolecular forces.<sup>9–14</sup>

In the latter, the resulting, well-ordered polymer patterns possess an average spacing governed by the wavelength of the fastest growing mode associated with the initial perturbation that triggered the instability, the so-called *most dangerous wavelength*  $\lambda_m$ , which dominates the initial stages of the pattern formation process prior to the onset of nonlinear effects. For smooth substrates, linear stability theory suggests only those fluctuations with a wavelength larger than a critical cutoff  $\lambda_c$  will grow in amplitude over time. The most dangerous wavelength

may then be determined,<sup>15,16</sup> that is,  $\lambda_m = \lambda_c/2^{1/2}$ , though the dependence of the cutoff wavelength  $\lambda_c$  on the fluid film characteristics reveals the difficulty of controlling the spacing of the pattern through manipulation of the fluid alone without the use of templating procedures.

We show here, however, that it is possible to obtain polymer patterns ordered over long distances with controlled spacing and spot sizes by driving the interfacial destabilization of a thin polymer fluid film with surface acoustic waves (SAWs), electroelastic Rayleigh waves that propagate along the surface of a piezoelectric substrate at amplitudes of a few nanometers.<sup>17</sup> We have already demonstrated the use of such devices for rapid atomization<sup>18,19</sup> in addition to a host of other microfluidic processes.<sup>20–23</sup> We note that a related study has hinted at the possibility of using SAWs to drive dewetting of 50 nm spray coated polymer films,<sup>24</sup> but we did not observe any regular ordering in their patterning.

The SAW devices used in this work consist of a double port interdigital transducer (IDT) with 25 pairs of 400 nm thick, straight aluminum electrodes sputter-deposited onto a single crystal 127.68° yx-cut lithium niobate (LiNbO<sub>3</sub>, Roditi UK, London) piezoelectric substrate, as shown in Figure 1a. The IDT fabrication atop the piezoelectric substrate was performed using standard ultraviolet photolithography and wet etch. In order to generate the SAW, a sinusoidal electrical signal matching the operating frequency is applied to the IDT using a RF signal generator (Agilent N9310A) and RF power amplifier (Faraday Pty. Ltd. 10W1000C). The SAW, which travels from the IDT across the substrate, has a wavelength  $\lambda$  which is set by the IDT finger width and spacing, both of which are  $\lambda/4$ . This determines the frequency of the device,  $f = c_s/\lambda$ , where  $c_s \approx 3965$  m/s is the speed of the SAW in the substrate. By incorporating a reflector IDT at the opposite end (Figure 1a), a standing SAW can be produced between the IDTs, as shown in Figure 1b, confirmed

\* To whom correspondence should be addressed. Telephone: + 61 3 9905 3834. Fax: + 61 3 9905 4943. E-mail: leslie.yeo@eng.monash.edu.au.

(1) Yan, L.; Huck, W. T. S.; Zhao, X.-M.; Whitesides, G. M. *Langmuir* **1999**, *15*, 1208–1214.

(2) Li, H.-W.; Muir, B. V. O.; Fichet, G.; Huck, W. T. S. *Langmuir* **2003**, *19*, 1963–1965.

(3) Reiter, G. *Phys. Rev. Lett.* **1992**, *68*, 75–78.

(4) Higgins, A. M.; Jones, R. A. L. *Nature* **2000**, *404*, 476–478.

(5) Xie, R.; Karim, A.; Douglas, J. F.; Han, C. C.; Weiss, R. A. *Phys. Rev. Lett.* **1998**, *81*, 1251–1254.

(6) Redon, C.; Brochard-Wyart, F.; Rondelez, F. *Phys. Rev. Lett.* **1991**, *66*, 715–718.

(7) Sehgal, A.; Ferreiro, V.; Douglas, J. F.; Amis, E. J.; Karim, A. *Langmuir* **2002**, *18*, 7041–7048.

(8) Wang, J. Z.; Zheng, Z. H.; Li, H. W.; Huck, W. T. S.; Siringhaus, H. *Nat. Mater.* **2004**, *3*, 171–176.

(9) Kataoka, D. E.; Troian, S. M. *Nature* **1999**, *402*, 794–797.

(10) Warner, M. R. E.; Craster, R. V.; Matar, O. K. *Phys. Fluids* **2002**, *14*, 4040–4054.

(11) Yeo, L. Y.; Craster, R. V.; Matar, O. K. *Phys. Rev. E* **2003**, *67*, 056315.

(12) Gonuguntla, M.; Sharma, A. *Langmuir* **2004**, *20*, 3456–3463.

(13) Bormashenko, E.; Pogreb, R.; Stanevsky, O.; Bormashenko, Y.; Stein, T.; Gengelman, O. *Langmuir* **2005**, *21*, 9604–9609.

(14) Wu, N.; Pease, L. F., III; Russel, W. B. *Langmuir* **2005**, *21*, 12290–12302.

(15) Vrij, A. *Discuss. Faraday Soc.* **1966**, *42*, 23–33.

(16) Sharma, A.; Ruckenstein, E. J. *Colloid Interface Sci.* **1986**, *113*, 456–479.

(17) White, R.; Voltmer, F. *Appl. Phys. Lett.* **1965**, *7*, 314–316.

(18) Friend, J. R.; Yeo, L. Y.; Arifin, D. R.; Mechler, A. *Nanotechnology* **2008**, *19*, 145301.

(19) Qi, A.; Friend, J. R.; Yeo, L. Y. *Phys. Fluids* **2008**, *20*, 074103.

(20) Tan, M. K.; Friend, J. R.; Yeo, L. Y. *Lab Chip* **2007**, *7*, 618–625.

(21) Li, H.; Friend, J. R.; Yeo, L. Y. *Biomaterials* **2007**, *28*, 4098–4104.

(22) Shilton, R.; Tan, M. K.; Yeo, L. Y.; Friend, J. R. *J. Appl. Phys.* **2008**, *104*, 014910.

(23) Li, H.; Friend, J. R.; Yeo, L. Y. *Phys. Rev. Lett.* **2008**, *101*, 084502.

(24) Grate, J. W.; McGill, R. A. *Anal. Chem.* **1995**, *67*, 4015–4019.

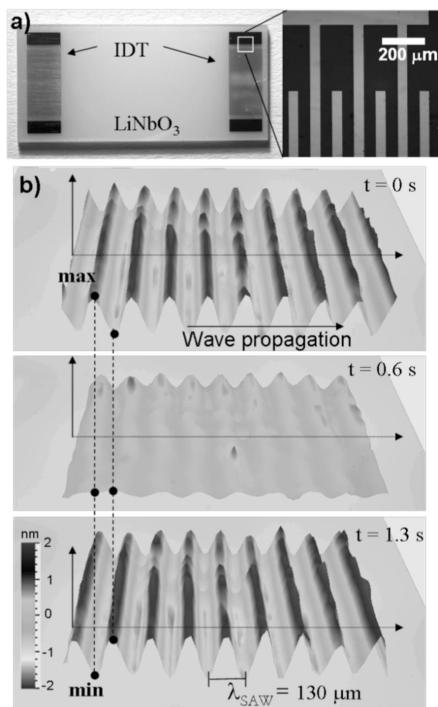


**Figure 1.** (a) Image of a typical SAW device. The inset shows a magnification of the fabricated IDT electrodes patterned via photolithography onto the piezoelectric substrate. (b) Time sequence images of the SAW for a 30 MHz device indicating the presence of a transverse traveling wave component, acquired using a laser Doppler vibrometer.

by laser Doppler vibrometry (Polytec MSA-400) scans of the transverse SAW component along the surface of the substrate. We note that a slight traveling wave component is still present: the standing wave ratio (SWR) is calculated to be around 4.9 (SWR = 1 corresponds to a pure standing wave, and SWR  $\rightarrow$   $\infty$  corresponds to a pure traveling wave).

The model fluid, on the other hand, consisted of poly- $\epsilon$ -caprolactone (PCL,  $M_w$  65 000, Sigma-Aldrich) dissolved in acetone (at 1% w/v). The polymer solution was delivered onto the substrate surface in the form of a drop with the use of a syringe pump (KD Scientific) at flow rates of 1 mL/h, connected to a hypodermic syringe needle placed just above but not in contact with the substrate (Figure 2). Imaging of the drop translation, film atomization, and polymer pattern formation was carried out at 2000 frames/s using a high-speed digital camera (Mikrotron MC1310) connected to a long distance microscope (Infinity, CO).

Due to the traveling wave component of the SAW, as evident in the laser Doppler vibrometry scans in Figure 1b, the SAW propagates along the substrate until it comes into contact with a liquid drop of polymer solution periodically dispensed onto the substrate. At this time, the axially polarized component of the SAW refracts into the liquid as a bulk sound wave at an angle known as the Rayleigh angle,  $\theta_R = \sin^{-1}(c_f/c_s)$ , due to the difference in the sound velocity in the substrate  $c_s$  and in the liquid  $c_f$ , as shown in Figure 2a. With sufficient amplitude of the incident SAW radiation, the sound wave in the fluid will have sufficient intensity to give rise to compressibility and therefore density variations in the fluid that are spatially out of phase with the pressure field in the bulk sound wave.<sup>20</sup> This gives rise to *acoustic streaming* in and a net body force on the drop, which, in turn, causes the drop to translate in the direction of the SAW propagation (Figure 2b) at around 1–10 mm/s order velocities,<sup>20</sup> leaving behind a trailing thin film layer that is typically 10  $\mu$ m

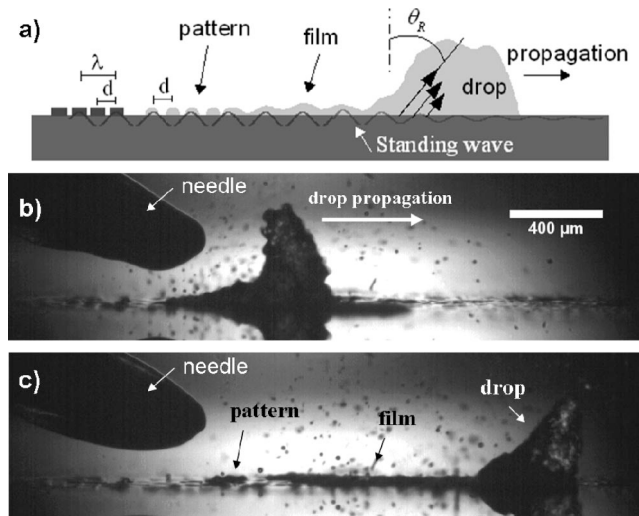


**Figure 2.** (a) Schematic illustrating the propagation of the SAW along the substrate and its diffraction into a drop at the Rayleigh angle  $\theta_R$ , giving rise to a net body force on the drop that causes it to translate in the direction of the SAW propagation, leaving behind it a thin film. (b,c) Image acquired using a high-speed camera showing (b) the distortion and translation of the drop and (c) the trailing film behind the drop and the initial stages of the pattern formation process as the film thins and depletes.

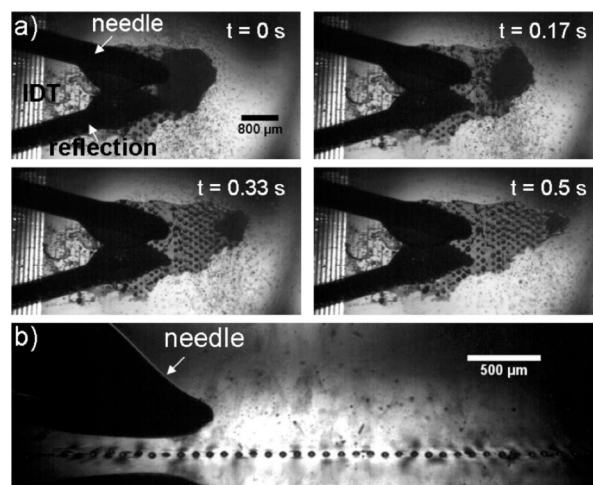


**Figure 3.** (a) Sequence of images (top view) depicting the translation of the drop and the formation of a thin film behind it, which, while being atomized, subsequently thins and depletes to produce a two-dimensional array of polymer droplets on the substrate. (b) Lateral view of the polymer patterns obtained through a 20 MHz SAW device.

in thickness (Figure 2c). The volume of solution displaced, velocity, and film thickness depend on the applied power. This entire process is captured through high-speed imaging in movie S1 in the Supporting Information.

Due to the high surface acceleration produced by the SAW, typically  $10^7$  m/s<sup>2</sup>, capillary waves are induced at the free surfaces of the drop and thin trailing film, as seen in Figure 2. We have shown in a previous study<sup>19</sup> that, for very thin films similar to those obtained here, the interface vibrates at a resonance frequency associated with a capillary–inertia force balance that is on the same order as the SAW frequency  $f$  ( $\sim 10$ – $10^2$  MHz). Further, the capillary waves possess similar wavelengths to those of the SAWs.

The interface is rapidly destabilized by the large accelerations, leading to atomization of the film with peaks in the capillary undulations pinching off to form jets and droplets. Previous studies

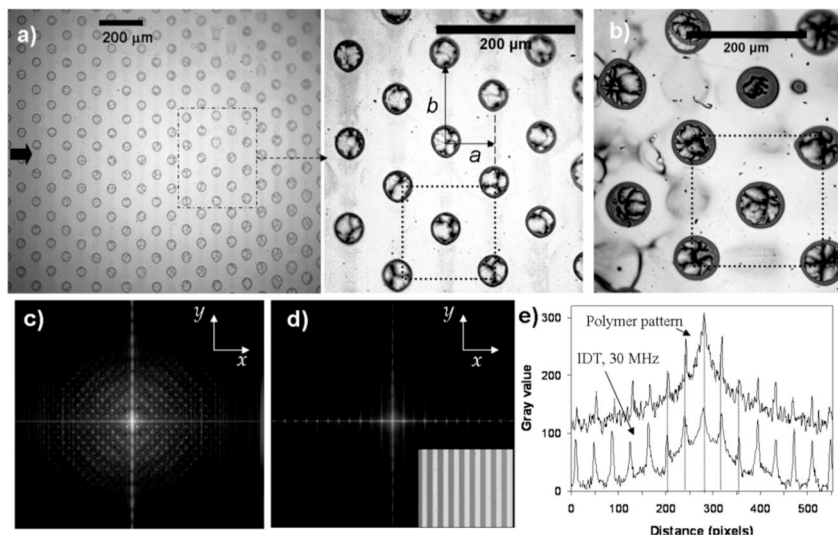


**Figure 4.** Periodically ordered polymer patterns obtained using (a) 30 MHz SAW irradiation (and its magnification at the right) and (b) a 20 MHz device. The SAW propagation direction is from left to right. FFT of (c) the patterns obtained with a 30 MHz device and (d) the IDT of a 30 MHz device (the scale of the IDT is shown in the inset). (e) The intensities of the FFT of (c) the pattern and (d) the IDT along the  $x$ -axis (for  $y = 0$ ) are strongly correlated (an offset was introduced to distinguish between both curves).

using laser Doppler vibrometry to measure the free surface have revealed large destabilization amplitudes of the capillary waves at the free surface, which are almost on the same order as the film thickness.<sup>19,23</sup> Here, the thinning regions are located at fixed distances from the output end of the source IDT, with each distance an integer multiple of one-half the SAW wavelength in the substrate, corresponding to the antinodes of vibration transverse to the substrate in the standing wave established between the driven and reflector IDTs. It is thus conceivable and likely that the film is thinned at the troughs of these capillary waves as a consequence of the violent free surface vibrations at these antinodes (especially in comparison to the relatively quiescent conditions at the nodes). Due to the large destabilization amplitudes, the thinning at the troughs occurs to a point beyond which stabilizing capillary stresses are no longer able to counterbalance the growing van der Waals force and the film ruptures. The film thinning and depletion due to the capillary undulations is also compounded by the evaporation of the solvent, the rate of which is locally enhanced where there is significant thinning of the film.

The breakup of the film across its entire surface due to its depletion or rupture at the antinodal positions, both axially and transversely, produces evenly spaced polymer droplets. The droplets solidify into the spot patterns observed in Figure 3 as the solvent evaporates (see also Figure S1 in the Supporting Information). Overall, the process is quite dramatic, as shown by movie S2 in the Supporting Information obtained using high-speed imaging. We note that the translation of the drop and the generation and subsequent atomization of the trailing film (hence the requirement for a traveling wave component of the SAW) are necessary conditions for the production of the polymer patterns. As such, there exists a threshold power associated with the onset of drop translation and subsequent formation of the patterns.

Figure 4 shows the polymer patterns obtained for both 20 and 30 MHz devices. In every case, the polymer spots are regularly ordered in a two-dimensional hexagonal close-packed lattice over a coverage of 1–5 mm<sup>2</sup>. The close packing occurs as a consequence of energy minimization requirements that permit maximum separation between the droplets, which stipulate that the transverse pitch  $b$  be twice that of the longitudinal pitch  $a$ .

**Table 1. Spot Diameter  $D$ , Longitudinal Pitch Spacing  $a$ , and Transverse Pitch Spacing  $b$  of the Polymer Patterns Observed for Various SAW Devices with Different Frequencies  $f$  and Hence Wavelengths  $\lambda$**

$f$ [MHz]	$\lambda$ [ $\mu\text{m}$ ]	$D$ [ $\mu\text{m}$ ]	$a$ [ $\mu\text{m}$ ]	$b$ [ $\mu\text{m}$ ]
8.86	400	145 $\pm$ 9	205 $\pm$ 22	392 $\pm$ 37
19.37	200	71 $\pm$ 3	103 $\pm$ 6	194 $\pm$ 5
30.38	130	36 $\pm$ 2	63 $\pm$ 3	125 $\pm$ 4
48.56	80	23 $\pm$ 4	39 $\pm$ 3	72 $\pm$ 7

Further inspection of the patterns produced with devices with different SAW frequencies reveals that  $a$  is always approximately equal to  $\lambda/2$  and hence  $b$  is approximately equal to  $\lambda$  (see Table 1). The fast Fourier transform (FFT) of the pattern (Figure 4d) is characterized by high-intensity Bragg peaks along the  $x$ -axis ( $y = 0$ ) and a “spinodal ring”, whose symmetry indicates the hexagonal tessellation in the pattern and reveals a high degree of perfection with negligible defect concentration. In Figure 4e, we observe the profiles along the  $x$ -axis at  $y = 0$  of the FFT associated with the patterns in Figure 4a, given by Figure 4c, and the FFT of the IDT (30 MHz device) depicted in Figure 4d show the strong coupling between the polymer pattern lattice and the IDT periodicity (or the SAW wavelength  $\lambda$ ). The close correlation of  $a$ ,  $b$ , and  $D$  with the device frequency  $f$  and hence  $\lambda$  (and, consequently, the instability wavelength) is shown in Figure 5, from which linear regression reveals slopes for  $a$ ,  $b$ , and  $D$  of 1.00, 0.52, and 0.39, respectively, with regression coefficients of 0.999 for  $b$  and 0.998 for both  $a$  and  $D$ .

It is interesting to note that the rapid evaporation of the solvent also drives a thermodynamic instability that results in spatial nonuniformities in the polymer and solvent concentration within the drop. Consequently, the existence of solvent-rich and polymer-rich regions results in “bubblelike” internal structures within the polymer spots, as observed in Figure 4b, reminiscent of the morphologies resembling grape bunches on the surface of the nanoparticles synthesized through a similar SAW-driven atomization process.<sup>18</sup>

In any case, the results above highlight the possibility of a rapid and highly controllable method for self-organized regular spatial polymer pattern formation through local thin film depletion as a consequence of violent interfacial destabilization driven by surface acoustic waves. A key attraction that this process offers

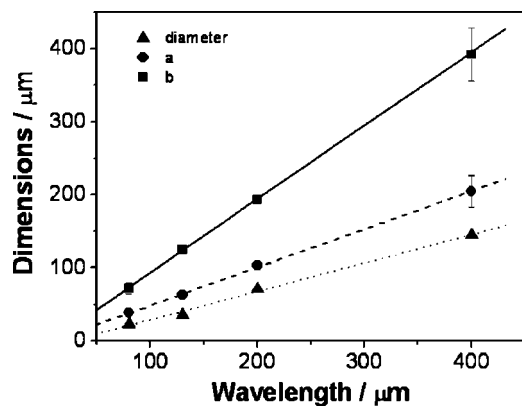


**Figure 5.** Dependence of the spot diameter  $D$ , the longitudinal pitch spacing  $a$ , and the transverse pitch spacing  $b$  of the polymer patterns on the device frequency  $f$  and hence the SAW wavelength  $\lambda$  (see Table 1).

over other methods is its ability for tuning the pattern periodicity as well as the polymer spot size merely through a single parameter, namely, the SAW frequency (or wavelength), without the necessity for surface treatment or templating.

**Acknowledgment.** This work was supported by the Australian Research Council (Discovery Projects DP0666660 and DP0773221). We are also grateful to an anonymous referee for his or her insightful comments on the manuscript.

**Supporting Information Available:** Figure S1 (File002): Image capturing the initial stages of the polymer spot pattern formation. The film has depleted at interstitial positions to leave behind residual droplets, the evaporation of which results in the formation of polymer spots. Movie S1 (File 003): A drop that is deposited onto the substrate of the device translates rapidly across due to the action of the surface acoustic wave. Note the deformation of the drop into a conical shape, which leans in the direction of the surface acoustic wave propagation at an angle defined by the Rayleigh angle. The translating drop leaves behind a thin trailing film. It is this film that eventually thins and depletes to form droplets which subsequently evaporate to form the polymer spots (see Movie S2). Movie S2 (File004): Rapid interfacial destabilization and atomization of the trailing thin film due to the surface acoustic wave. The film eventually depletes or ruptures to form residual droplets on the substrate, which eventually evaporate to form the polymer spots. Note the homogeneity in the spacing of the residual droplets at the end of the movie. In this case, the translating drop (Movie S1) is not present. This material is available free of charge via the Internet at <http://pubs.acs.org>.

LA802255B